Science of the Total Environment 770 (2021) 145364

Contents lists available at ScienceDirect

Science of the Total Environment

journal homepage: www.elsevier.com/locate/scitotenv

Phosphate removal using surface enriched hematite and tetra-n-butylammonium bromide incorporated polyacrylonitrile composite nanofibers

Chengshuang Wang [a,b], Sooyoun Yu [b], David M. Cwiertny [c], Yadong Yin [d], Nosang V. Myung [b,e,*]

[a] School of Materials Science and Engineering, Yancheng Institute of Technology, Yancheng 224051, China
[b] Department of Chemical and Environmental Engineering, University of California, Riverside, CA 92521, USA
[c] Department of Civil and Environmental Engineering, University of Iowa, Iowa City, IA 52242, USA
[d] Department of Chemistry, University of California, Riverside, CA 92521, USA
[e] Department of Chemical and Biomolecular Engineering, University of Notre Dame, Notre Dame, IN 46556, USA

HIGHLIGHTS

- Hematite and TBAB enriched on surface of PAN composite nanofibers
- Surfactant-mediated electrospinning controlled diameter and composition of nanofibers
- The phosphate removal by the chemisorption on surface-enriched Fe_2O_3 nanoparticles
- The maximum phosphate removal capacity was approx. 8.76 mg/g at pH 3
- Excellent reusability of the synthesized nanofiber membrane

GRAPHICAL ABSTRACT

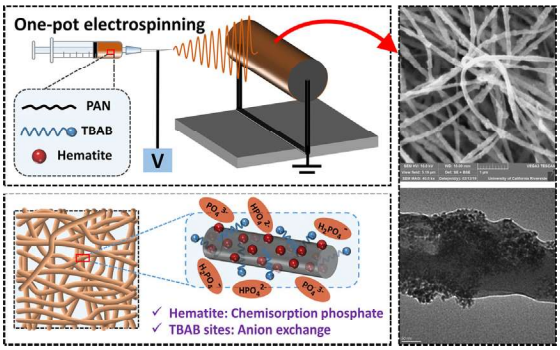

ARTICLE INFO

Article history:
Received 22 November 2020
Received in revised form 27 December 2020
Accepted 18 January 2021
Available online 24 January 2021

Ediotr: Jay Gan

Keywords:
Electrospinning
Nanofiber mat
Surfactant-mediated
Phosphorus removal

ABSTRACT

The nanosized iron oxides-based adsorbent has been widely used to alleviate water eutrophication. However, it is challenging to industrialize the application of nanosized iron oxides-based adsorbent due to their poor stability, difficult separation and recovery.

Herein, hematite and tetra-n-butylammonium bromide incorporated polyacrylonitrile (PAN/Fe_2O_3/TBAB) composite nanofibers with a controlled diameter (i.e., 66 to 305 nm) and composition were systematically synthesized as an adsorbent for phosphate removal from water using surfactant-mediated electrospinning. During the electrospinning process, polar TBAB surfactant enhanced the migration of Fe_2O_3 nanoparticles toward the surface of nanofibers resulting in Fe_2O_3 nanoparticles/TBAB surface enriched nanofibers. The synthesized nanofiber membranes were used for phosphate removal, and their adsorption kinetics, adsorption mechanism, and reusability were investigated. Data showed that adsorption kinetic followed the pseudo-second-order model whereas the adsorption mechanism follows the Langmuir model. The phosphate removal was mainly derived from the chemisorption of surface-enriched α-Fe_2O_3 nanoparticles at acidic and circumneutral pH values, with a small contribution from anion exchange at TBAB sites. The maximum phosphate removal capacity was approx. 8.76 mg/g (i.e., 23.1 mg/g, P/active materials) at pH 3. Additionally, the synthesized nanofiber membrane also shows excellent reusability.

* Corresponding author at: Department of Chemical and Biomolecular Engineering, University of Notre Dame, Notre Dame, IN 46556, USA.
E-mail address: nmyung@nd.edu (N.V. Myung).

https://doi.org/10.1016/j.scitotenv.2021.145364
0048-9697/

1. Introduction

Phosphorus is one of the major nutrients for the growth of all life forms. However, excessive release of phosphorus through agricultural runoff and sewage discharge can cause undesirable eutrophication, which contributes to the death of aquatic species, algal blooms and parasite infection (Dodds et al., 2009; Fang et al., 2017). To recover the phosphorus resource and prevent this phenomenon, various remediation technologies such as chemical precipitation, biological uptake, ion exchange, and adsorption have been explored, and have demonstrated different degrees of remediation efficiency (Lalley et al., 2016; Liu et al., 2017; Nguyen et al., 2014; Xia et al., 2020). Among these remediation techniques, adsorption is one of the simplest, most effective and economical methods for wastewater purification (Cui et al., 2020; Singh et al., 2018).

Recently, nanosized metal oxides/hydroxides (e.g., Fe, Zn, Al, Mg, Ca, etc.) have been investigated for their potential for phosphorus removal because of their abundance, low cost, environmental friendliness, and chemically stability (Bacelo et al., 2020; Li et al., 2018; Lofrano et al., 2016; Tan et al., 2016; Zhao et al., 2018; Zhao et al., 2011). Although the nanosized metal oxides/hydroxides have a high efficiency of phosphate removal due to their high affinity for phosphate, it is challenging to industrialize the application of nanosized metal oxides-based adsorbents due to their poor stability, difficult separation and recovery. Meanwhile, membrane filtration technology in water treatment needs high efficiency, low cost and mass-produced functional membranes (Suja et al., 2017; Zhao et al., 2017). Nanofiber based non-woven membranes have high interconnecting porosity with adjustable pore size, which can lead to very promising filtration capabilities in terms of permeability, selectivity, and low fouling (Li et al., 2020).

Nanofibers can be produced via several different methods, including drawing, template synthesis, phase separation, self-assembly, and electrospinning. Among these methods, electrospinning has become more popular due to its easy set-up, high-yield, scalable manufacturing process and the ability to tune nanofiber diameter, producing robust nanofiber membranes ideal for environmental application (Chen et al., 2020; Ding and Yu, 2014; Greenstein et al., 2019; Liao et al., 2018; Peter et al., 2016; Xue et al., 2017). Previously, we have discovered that the integration of surfactants and metal oxides into electrospun polymeric nanofibers yielded promising functional nanofibers for sequestration of common (oxy)anionic water pollutants. The quaternary ammonium salts like TBAB accumulated at the polymer-air interface during curing, resulting in surface enrichment of not only cationic quaternary ammonium binding sites but also Fe_2O_3 nanoparticles (Peter et al., 2017; Peter et al., 2018).

Herein, we demonstrated the surfactant TBAB could promote the enrichment of the commercial α-Fe_2O_3 nanoparticles to the PAN nanofiber surface via a one-pot electrospinning technique. The resulting PAN/Fe_2O_3/TBAB nanofiber membranes displayed surface-enriched active binding agents (i.e., Fe_2O_3 nanoparticles and TBAB), low bead density, and exhibited a balance of high adsorption capacity for phosphate and adequate mechanical property. The adsorption behaviors of the PAN/Fe_2O_3/TBAB nanofiber membranes were evaluated by adsorption kinetics and equilibrium isotherm models. The pH effect on the phosphate removal efficiency, adsorption mechanisms and reusability of PAN/Fe_2O_3/TBAB nanofiber membranes were investigated to determine their potential for phosphate removal and recovery.

2. Materials and methods

2.1. Reagents

Polyacrylonitrile (PAN; M_W = 150,000), tetra-n-butylammonium bromide (TBAB; ≥98%), and potassium antimony tartrate hydrate (≥99%) were purchased from Sigma-Aldrich. Iron oxide (99.95%, 3 nm APS powder, S.A. 250 m^2/g), iron oxide nanorods (α-Fe_2O_3, 98%, 30–50 nm APS powder) and ammonium molybdate tetrahydrate (99%) were purchased from Alfa Aesar. Potassium dihydrogen phosphate (KH_2PO_4; 99.3%), *N*, *N*-dimethylformamide (DMF; 99.9%), sulfuric acid, ascorbic acid (99.4%), hydrochloric acid and sodium hydroxide were obtained from Fisher Chemical. All reagents were used as received without further treatment.

2.2. Preparation of PAN/Fe_2O_3/TBAB nanofiber mats

PAN/Fe_2O_3/TBAB nanofiber mats were fabricated by the electrospinning technique (Yu and Myung, 2018). The detailed procedure is as follows: Fe_2O_3 nanoparticles (~3 nm) or Fe_2O_3 nanorods were added to DMF and then dispersed under ultrasonic treatment for 1 h at 0.86–3 wt% relative to the total solution mass. PAN (4–7 wt%) and TBAB (1 wt%) were added to the vial containing either pure DMF or the abovementioned Fe_2O_3-DMF dispersions, which was then sealed for magnetic stirring in a water bath at 60 °C for 2 h. Then, the composite solutions were stirred at room temperature for 12 h to obtain the electrospinning solution.

Electrospinning was conducted by injecting the prepared solution through a 5-mL BD Luer-Lok syringe with a 25-gauge stainless steel needle, using a syringe pump (New Era, NE-100). Negative voltage was applied to the needle tip, while the drum collector wrapped with aluminum foil, rotating at 420 rpm, was grounded to collect the sample. Electrospinning and environmental conditions such as applied voltage, feed rate, temperature, and absolute humidity were fixed at 16 kV, 0.5 mL/h, 25 ± 1 °C, 0.0064 ± 0.0008 kg H_2O/kg dry air, respectively. Hereafter, the as-prepared PAN/Fe_2O_3/TBAB nanofiber mats derived from α-Fe_2O_3 nanoparticles were referred to as "PAN*x*-Fe_2O_3*y*-TBAB1" and the PAN/Fe_2O_3/TBAB nanofiber mats derived from α-Fe_2O_3 nanorods were referred to as "PAN*x*-Fe_2O_3(nanorods)*y*-TBAB1" where *x* and *y* denote PAN and Fe_2O_3 loadings, respectively.

2.3. Characterization

2.3.1. Electrospinning solution properties

For studying the effect of variable solution conditions on the resulting nanofiber properties, three solution properties – viscosity, surface tension, electrical conductivity – were measured. The viscosity was measured using a rotational Brookfield viscometer (DV-I Prime, Brookfield Engineering Laboratories, USA) at 23 °C. The surface tension was tested by an automatic surface tensiometer (QBZY-1, Shanghai Fangrui Instrument Co., Ltd., China) with a Wilhelmy small platinum plate at 23 °C. The electrical conductivity was measured using a glass-body electrical conductivity probe (K = 0.1, Oakton) paired with an embedded conductivity circuit (EZO-EC™, Atlas Scientific) at 23 °C. All measurements were repeated three times and then averaged. Solution properties were measured immediately before or after electrospinning to most closely correlate them to nanofiber properties.

2.3.2. Nanofiber morphology

The morphology including dimensions and bead (defect) density of the nanofiber mats were observed through a scanning electron microscope (SEM, VEGA3, TESCAN Ltd., Czech Republic) with a 10 kV acceleration voltage. The nanofiber mats were coated with a thin layer of gold by Electron Microscopy Sciences 575-X sputter at 20 mA (current) for 30 s before observation. SEM images were used to measure the nanofiber diameter, which was averaged over 50 unique measurements, as well as the bead density concerning the area of the SEM image obtained. Transmission electron microscopy (TEM) samples were collected by placing a carbon-coated copper grid directly in front of the drum collector for 1 min during electrospinning. TEM images were captured using FEI/Philips Tecnai12 TEM (FEI Company, USA) at 120 kV.

2.4. Batch adsorption experiments

To evaluate the efficiency of PAN/Fe_2O_3/TBAB nanofiber membranes for adsorption of phosphate, kinetics studies were carried out using 40 mg of the PAN-based nanofiber membranes in 40 mL of phosphate solution with initial pH of 5.6 and concentration of 2, 5, 10, 15 and 20 mg/L, respectively. The experiment was performed in a 50-mL sealed polypropylene centrifugal tube at 23 °C. The solution was collected using a 5-mL BD Luer-Lok syringe with a syringe filter attached (0.22 μm, PTFE Teflon filter) at different time intervals (0.25, 0.5, 1, 2, 4, 8 and 24 h). The phosphate concentration of collected samples was measured at 880 nm with a UV–vis spectrophotometer (Agilent Cary 60) based on the ascorbic acid molybdate blue method (Doolittle, 2014).

2.4.1. Effect of pH

The effect of initial pH was tested using a similar procedure at an initial phosphate concentration of 10 mg/L and adsorbent dosage of 1 g/L. The pH of phosphate solutions was adjusted to the desired values ranging from 2 to 13 by adding 0.1 M HCl or NaOH solution. Then, the PAN/Fe_2O_3/TBAB nanofiber membranes were immersed into the centrifuge tubes containing the phosphate solutions, which were sealed then gently shaken.

2.4.2. Adsorption kinetics and isotherm experiments

The equilibrium adsorption experiments were individually carried out in 2, 5-, 10-, 15-, and 20-mg/L phosphate solutions with 1 g/L PAN/Fe_2O_3/TBAB nanofiber mat at an initial pH of 5.6. The phosphate equilibrium adsorption capacity (q_e) was calculated by the following equation:

$$q_e = \frac{(C_0 - C_e) \times V}{m} \quad (1)$$

where q_e (mg/g) is the adsorption capacity at time t; C_0 and C_e are the initial and equilibrium phosphate concentration in the solution (mg/L), respectively; V is the volume of the solution (L); and m is the adsorbent amount (g).

The adsorption performances of nanofiber membranes were investigated using the pseudo-first-order and the pseudo-second-order equations (Eqs. (2) and (3))

$$q_t = q_e \times (1 - exp(-k_1 t)) \quad (2)$$

$$t/q_t = 1/(k_2 q_e^2) + t/q_e \quad (3)$$

where k_1 is the rate constant of pseudo-first-order adsorption (min^{-1}); k_2 is the rate constant of pseudo-second-order adsorption ($g \cdot mg^{-1} \cdot min^{-1}$); q_e is the amount of phosphate adsorption at equilibrium (mg/g); q_t is the amount of phosphate adsorption at time t (min) in mg/g.

The adsorption isotherms of nanofiber membranes were investigated using the Langmuir and Freundlich adsorption models (Eqs. (4) and (5))

$$C_e/q_e = 1/(K_L q_{max}) + C_e/q_{max} \quad (4)$$

$$\ln q_e = \ln K_F + (1/n) \ln C_e \quad (5)$$

where q_{max} is the maximum adsorption capacity in mg/g; C_e is the equilibrium phosphate concentration in mg/L; n is the parameter of the Freundlich adsorption isotherm; and K_L (L/mg) and K_F are the equilibrium constants related to the Langmuir and Freundlich adsorption isotherms, respectively.

2.4.3. Desorption experiments

To study the reusability and recovery of the PAN/Fe_2O_3/TBAB nanofiber membranes, the phosphate desorption experiment was carried out using alkaline regeneration. Firstly, the equilibrium adsorption experiments were carried out with 10 mg/L phosphate solutions and 1 g/L PAN5.5-$Fe_2O_3$2.36-TBAB1 nanofiber mat at an initial pH of 3 and 5. After the phosphate adsorption, the nanofiber mat was regenerated in the 1 M NaOH solution for 2 h. Then the mat was immersed in distilled water for 20 h, during which the water was replenished with fresh distilled water every 5 h. The resulting PAN5.5-$Fe_2O_3$2.36-TBAB1 nanofiber mat was dried at 60 °C, completing the 1st regeneration cycle. The five cycles of adsorption-desorption experiments were performed by repeating the same procedure.

3. Results and discussion

3.1. Design of experiment (DOE) analyses

Systematic variation of working conditions for electrospinning Fe_2O_3-embedded nanofibers was performed using a two-factor, three-level design of experiment (DOE). The two factors were PAN content in wt% and PAN-to-Fe_2O_3 ratio by wt%; the low and high levels of each factor were fixed at 4 and 7 wt% PAN and 1:0 to 3:7 PAN: Fe_2O_3, respectively, while the middle level was fixed at the median of the range. All sample names derived from this DOE, along with their solution and nanofiber properties, are summarized in Table 1.

3.1.1. Effect of solution conditions on solution properties

DOE methodology was employed to first identify and rank the effects of the two factors on the resulting solution properties like viscosity, surface tension, and electrical conductivity. DOE analysis of viscosity, surface tension, and electrical conductivity as a function of solution compositions are shown in Fig. 1. The viscosity of solutions increased sharply with the increase of both PAN concentrations and Fe_2O_3/PAN ratios. Notably, the effect degree of PAN concentration was bigger than that of iron oxide. This was attributed to the polymer concentration

Table 1
Effect of solution compositions on the solution and nanofiber properties.

Sample	Solution properties			Nanofiber properties	
	Viscosity (cP)	Surface tension (dynes/cm)	Electrical conductivity (μS/cm)	Average fiber diameter (nm)	Bead density (bead/μm^2)
PAN4-TBAB1	23.7 ± 1.2	36.0 ± 0.1	1176 ± 4	66 ± 16	2.0
PAN4-$Fe_2O_3$0.86-TBAB1	29.3 ± 2.3	36.8 ± 0.05	1155 ± 6	188 ± 31	0.002
PAN4-$Fe_2O_3$1.72-TBAB1	38.6 ± 2.6	35.9 ± 0.1	1149 ± 8	71 ± 15	1.51
PAN5.5-TBAB1	55.4 ± 3.1	36.9 ± 0.03	1040 ± 7	149 ± 29	0.01
PAN5.5-$Fe_2O_3$1.18-TBAB1	75.8 ± 3.6	36.8 ± 0.03	1033.5 ± 13	90 ± 22	0.54
PAN5.5-$Fe_2O_3$2.36-TBAB1	107 ± 6.9	37.3 ± 0.1	1130 ± 8	147 ± 32	0.009
PAN7-TBAB1	141 ± 3.7	37.2 ± 0.1	939 ± 2.5	157 ± 34	0.014
PAN7-$Fe_2O_3$1.5-TBAB1	259 ± 2.7	37.2 ± 0.1	918.1 ± 7	273 ± 41	0.001
PAN7-$Fe_2O_3$3-TBAB1	817.2 ± 8	37.3 ± 0.03	911.1 ± 9	305 ± 48	0

being the key factor to affect the chain entanglement. When the polymer concentration increased, polymeric chains reduced in mobility in solution due to chain entanglement formation, which prevented the chain re-ordering and raised the solution viscosity (Chisca et al., 2012).

When high voltage is applied during electrospinning, the solution becomes highly charged, and as a result, the solution droplet at the tip will experience two major types of forces, the electrostatic repulsion force and surface tension. Because nanofibers will only form when the electrostatic repulsion exceeds that of the surface tension in the solution, controlling the surface tension is also critical in achieving electrospinning stability (Xue et al., 2019). As shown in Fig. 1b, the surface tension of the solution generally remained at a level of 36.8 dynes/cm. As it is generally controlled by the presence or absence of a surfactant, surface tension was not affected by the PAN concentrations or Fe_2O_3/PAN ratios.

Typically, with the increase of the electric conductivity of the solution, there is a significant decrease in the diameter of the electrospun nanofibers. With low electrical conductivity of the solution, on the other hand, insufficient elongation of a jet by electric force may lead to the formation of beads (Bhardwaj and Kundu, 2010; Ding and Yu, 2014). The effect of solution conditions on the electrical conductivity of the solution shown in Fig. 1c exhibited unexpected behavior; it appears controlled solely by the concentration of the polymer, while the addition of the Fe_2O_3 nanoparticles had a negligible effect. This might be because a lower-viscosity solution allowed for higher mobility of the polar molecules (Ding and Yu, 2014; Xue et al., 2019), shown by

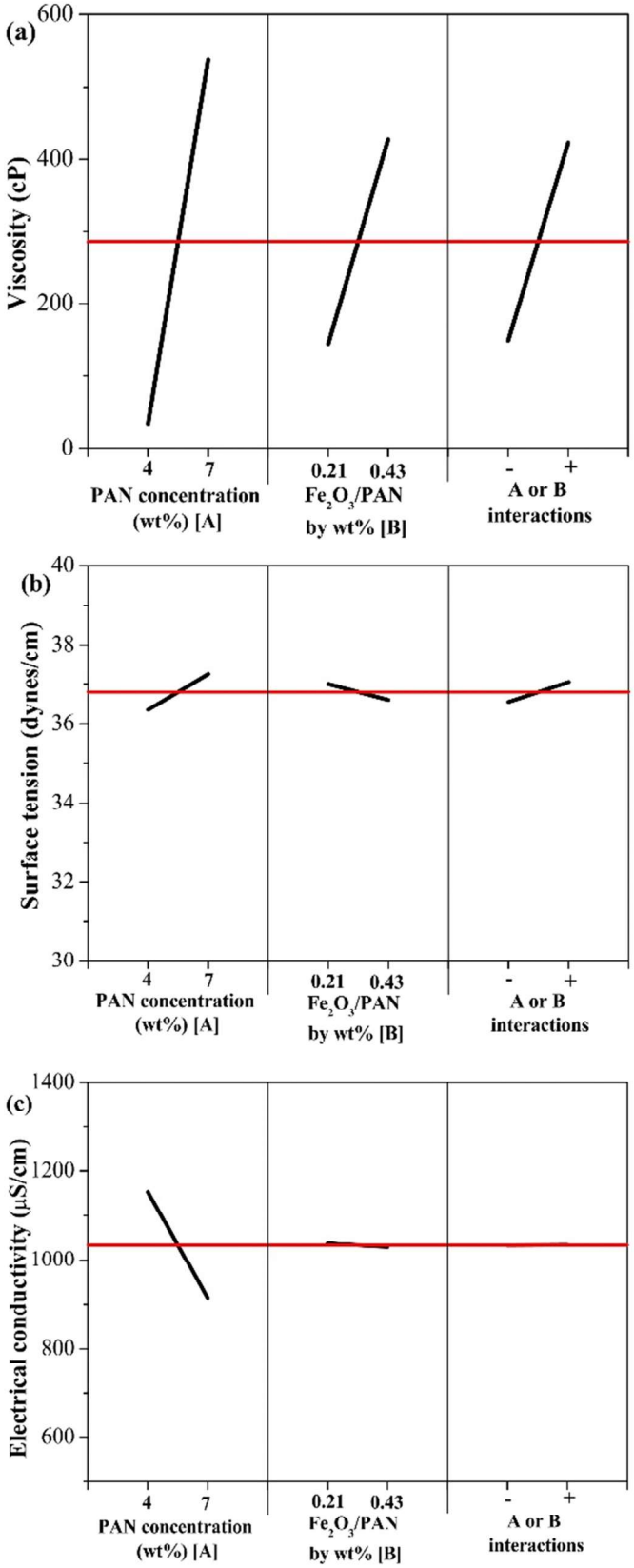

Fig. 1. DOE analysis of (a) viscosity (b) surface tension and (c) electrical conductivity as a function of solution compositions.

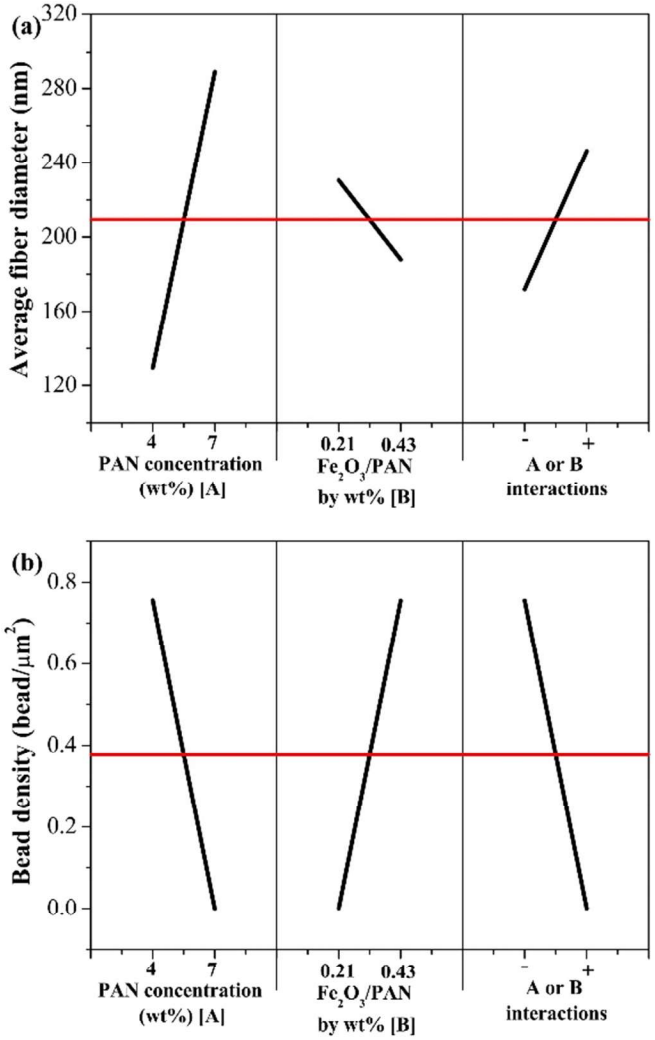

Fig. 2. DOE analysis of (a) average fiber diameter and (b) bead density as a function of solution compositions.

the electrical conductivity in the 1100s μS/cm for 4 wt% PAN-based solutions compared to that in 900s μS/cm for 7 wt% PAN-based solutions.

3.1.2. Effect of solution conditions on nanofiber morphology

A total of 9 solutions were electrospun under the same electrospinning and environmental conditions to study the effect of solution conditions on the resulting nanofiber properties – namely, the average nanofiber diameter and bead density, as well as the overall morphology. The SEM images of the PAN/Fe_2O_3/TBAB nanofiber mats are presented in Fig. 3, which can provide visual information from the topographic view. The images of SEM has been analyzed by ImageJ software to measure the diameter and bead density of nanofibers (Table 1). Control PAN nanofibers that did not contain TBAB exhibited average diameters of 88 ± 26 and 228 ± 37 nm for PAN4 and PAN7 nanofiber mats, respectively. With the introduction of 1 wt% quaternary ammonium salts (TBAB) to the electrospinning solution, the average diameter of the resulting nanofibers decreased to 66 ± 16 and 157 ± 34 nm, respectively. The average diameter of nanofiber mats increased with the increase of PAN concentration, which was expected as solution viscosity, largely controlled by polymer concentration, is a known contributor to nanofiber diameter. DOE analysis (Fig. 2) further showed that PAN concentration and Fe_2O_3/PAN ratios had a competing effect on the nanofiber average diameter and bead density. The higher PAN concentration would lead to higher nanofiber diameter and lower bead density, which could be attributed to the more stable formation of nanofiber jet with higher-viscosity solutions. Except for the two nanofiber samples (i.e., PAN4-$Fe_2O_3$1.72-TBAB1 and PAN5.5-$Fe_2O_3$1.18-TBAB1), the bead density of PAN/Fe_2O_3/TBAB nanofiber mats was lower than 0.009 bead/μm^2.

3.1.3. Effect of TBAB content on the physical properties of nanofiber mats

To demonstrate the surfactant TBAB function in the electrospinning procedure and the effect of Fe_2O_3 dimension on the properties of nanofiber mat, we selected two types of α-Fe_2O_3 (nanoparticles and nanorods) and different TBAB content (0, 0.1 and 1 wt%) to obtain the resulting nanofiber mats. The solution and nanofiber properties of nanofiber mats were listed in Table S1. The introduction of the surfactant TBAB in the polymer precursor solution will increase the electrical conductivity and decrease the viscosity of the solution. The SEM images of the PAN/Fe_2O_3/TBAB nanofiber mats were shown in Fig. S1. With the increase of surfactant TBAB content, the PAN/Fe_2O_3/TBAB nanofibers were more uniform and low bead density in the mat. Usually, beads are products of the instability of the jet under the electric field. The higher the charge density and the lower the surface tension, the bead formation is suppressed (Park et al., 2008). For the α-Fe_2O_3 nanoparticles, the change of viscosity of the polymer solution and charge density are the main factors to produce a

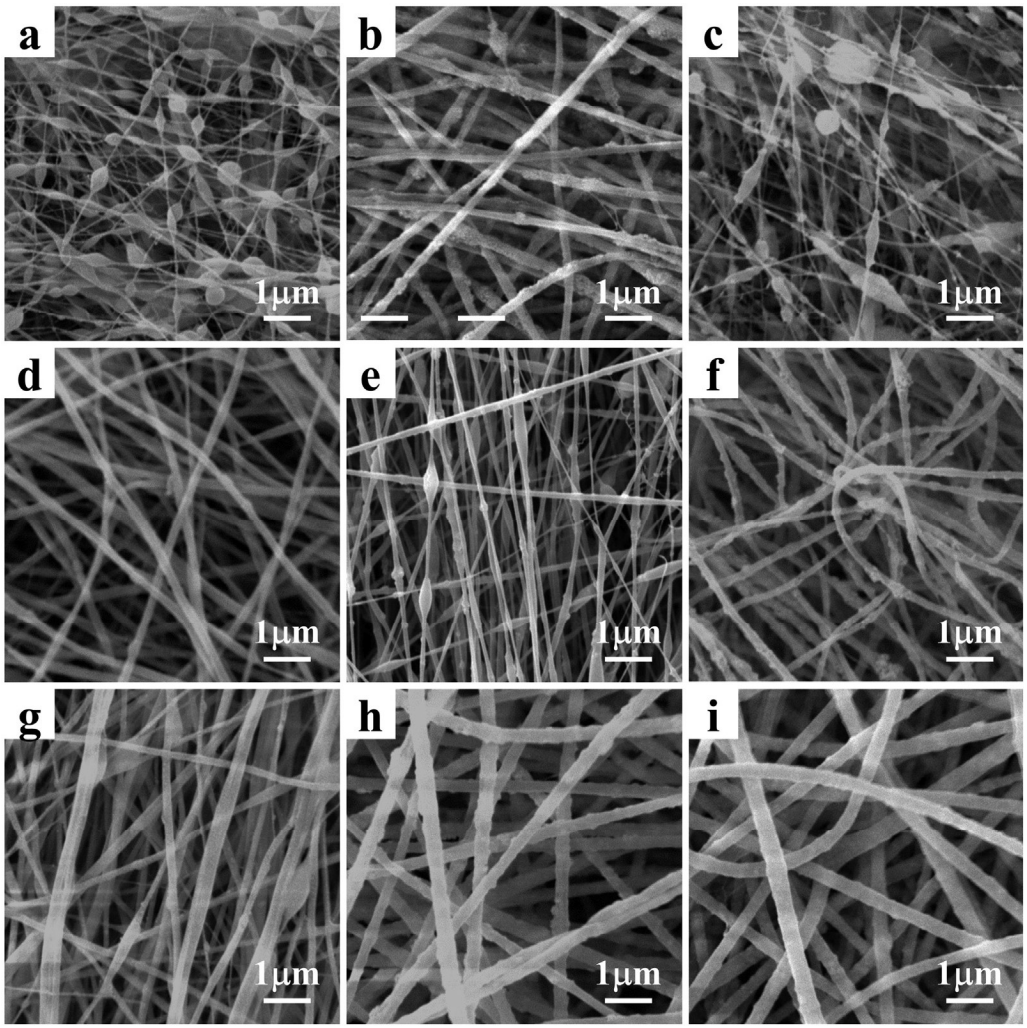

Fig. 3. SEM images of PAN/Fe_2O_3/TBAB nanofibers. (a) PAN4-TBAB1, (b) PAN4-$Fe_2O_3$0.86-TBAB1, (c) PAN4-$Fe_2O_3$1.72-TBAB1, (d) PAN5.5-TBAB1, (e) PAN5.5-$Fe_2O_3$1.18-TBAB1, (f) PAN5.5-$Fe_2O_3$2.36-TBAB1, (g) PAN7-TBAB1, (h) PAN7-$Fe_2O_3$1.5-TBAB1 and (i) PAN7-$Fe_2O_3$3-TBAB1.

trend of resulting high nanofiber diameter and low bead density. In comparison, the nanofiber of PAN5.5-Fe_2O_3(nanorods)2.36-TBAB1 presented the more smooth surface, uniform diameter and low bead density. When the introduction of 1 wt% TBAB, the resulting nanofiber mat with low bead density can be easy to handle and peel off to facilitate it applied to membrane filtration technology.

3.2. Nanofiber morphology

3.2.1. SEM

Morphological studies of the electrospun nanofiber mats were done using scanning electron microscopy, which provides visual information of the topographic view and the cross-sectional structure of the membrane. As shown in Fig. 3, the SEM image of the PAN/Fe_2O_3/TBAB nanofiber mats revealed randomly oriented three-dimensional nonwoven membranes with a uniform diameter ranging from 66 to 305 nm, which was a typical random deposition aggregate structure of electrospinning nanofibers. For a higher PAN concentration, PAN/Fe_2O_3/TBAB nanofibers were defect-free, because there were more PAN chain entanglements and less chain mobility hardening the jet extension, which reduced the disruptions during the electrospinning process, favoring the formation of large-diameter nanofibers. The SEM images in Fig. 3 were similar to the previous results (Peter et al., 2017) of surfactant-assisted dispersion of nanomaterials in the PAN nanofiber surface. PAN/Fe_2O_3/TBAB nanofiber surfaces appeared rough in Fig. 3, indicating the Fe_2O_3 nanoparticles were mostly present as aggregates, with some at or near the nanofiber surface. This was attributed to the interactions between the surfactant and Fe_2O_3 nanoparticles (e.g., formation of surfactant mono- or bi-layers on nanoparticle surfaces), which improved Fe_2O_3 dispersion and minimized clogging during solution injection.

3.2.2. TEM

For confirming the dispersion state of Fe_2O_3 within the PAN nanofiber, the Fe_2O_3 nanoparticles and PAN/Fe_2O_3/TBAB nanofibers were evaluated by TEM. A typical TEM image of α-Fe_2O_3 nanoparticles is shown in Fig. 4a, which was mostly aggregates of tiny particles (3 nm). The TEM images (Fig. 4b–d) of PAN/Fe_2O_3/TBAB nanofibers with the same Fe_2O_3/PAN ratio demonstrated the surface enrichment of Fe_2O_3 nanoparticles when used in tandem with surfactant TBAB, a phenomenon we previously observed for PAN composites containing surfactants (CTAB and TBAB) and ferrihydrite nanoparticles (Peter et al., 2017). This was attributed to nanoparticle–quaternary ammonium salts interactions; surface segregation of TBAB during electrospinning helped "pull" the Fe_2O_3 nanoparticles to the nanofiber surface and minimized free energy. Although aggregation of Fe_2O_3 nanoparticles was observed throughout the PAN/Fe_2O_3/TBAB nanofibers, most of the Fe_2O_3 nanoparticles were enriched at the surface of the nanofiber. Without surfactant TBAB, the TEM image (Fig. 4e) of PAN5.5-$Fe_2O_3$2.36 displayed most of the Fe_2O_3 nanoparticles were buried in the nanofiber. With the increase of surfactant TBAB content, most Fe_2O_3 nanoparticles have enriched the surface of the nanofiber. Surfactant TBAB medicated PAN/Fe_2O_3/TBAB nanofibers not only reduce bead density of nanofibers, but also increase the active binding agents like Fe_2O_3 nanoparticles and TBAB on the nanofiber surface. It was thus hypothesized that the active binding agents such as Fe_2O_3 nanoparticles and TBAB can come into direct contact with pollutants, thus improving the removal efficiency of pollutants when the as-spun PAN/Fe_2O_3/TBAB nanofiber mats are used in water treatment. As shown in Fig. 4h, the α-Fe_2O_3 nanorods are presented 30–50 nm length and several nanometers width. When introduction of 1 wt% TBAB in the PAN5.5-Fe_2O_3(nanorods)2.36-TBAB1 nanofibers (Fig. 4g), the α-Fe_2O_3 nanorods aggregation were aligned along nanofiber axis direction, not displayed the surface-segregation and just buried in the nanofibers. This is attributed to the high aspect ratio and asymmetric shape of α-Fe_2O_3 nanorods makes them aligned along the nanofiber axis while the nanofiber is pulled out from the syringe needle during electrospinning. So the phosphate removal efficiency of PAN5.5-Fe_2O_3(nanorods)2.36-TBAB1 nanofiber mats was low due to the active binding agents α-Fe_2O_3 nanorods buried in the nanofibers.

3.3. Adsorption kinetics

Phosphate removal in batch systems helps establish the equilibrium time and removal rate of phosphate from aqueous solution by the adsorbent. Two popularly used kinetic models, the pseudo-first-order and pseudo-second-order (Eqs. (2) and (3)) were used to fit the batch experiment data. The kinetics data of the phosphate adsorption onto different PAN/Fe_2O_3/TBAB nanofiber membranes at 23 °C and pH 5.6 are shown in Fig. S2 and Fig. 5. The kinetic processes of phosphate adsorption onto the PAN/Fe_2O_3/TBAB nanofiber membranes could be divided into two stages: relatively rapid adsorption during the first 2 h

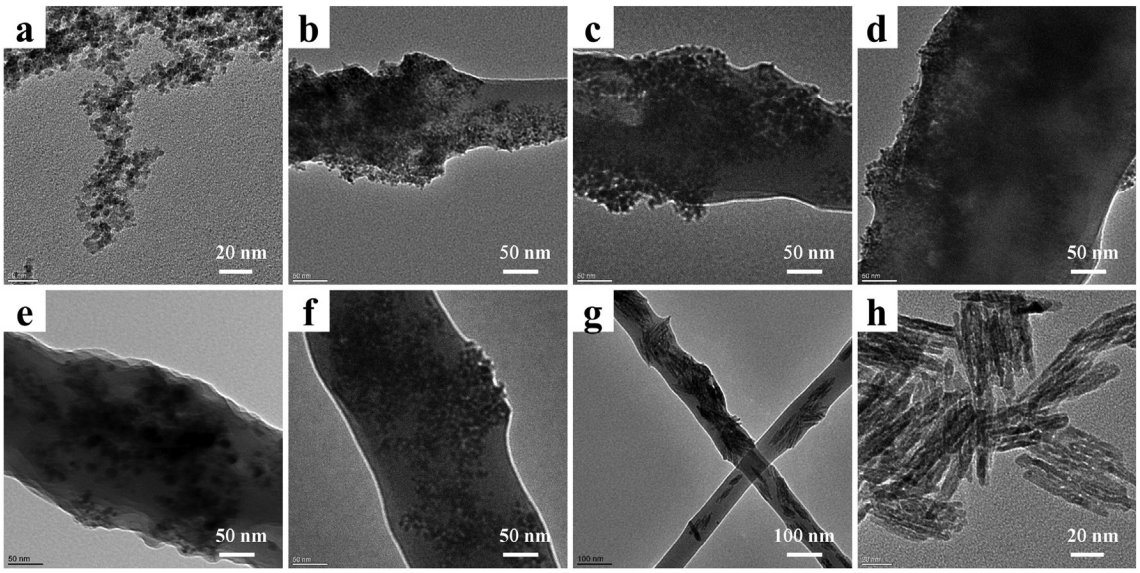

Fig. 4. TEM images of Fe_2O_3 nanoparticles, Fe_2O_3 nanorods and PAN/Fe_2O_3/TBAB nanofibers. (a) Fe_2O_3 nanoparticles, (b) PAN4-$Fe_2O_3$1.72-TBAB1, (c) PAN5.5-$Fe_2O_3$2.36-TBAB1, (d) PAN7-$Fe_2O_3$3-TBAB1, (e) PAN5.5-$Fe_2O_3$2.36, (f) PAN5.5-$Fe_2O_3$2.36-TBAB0.1, (g) PAN5.5-Fe_2O_3(nanorods)2.36-TBAB1 and (h) Fe_2O_3 nanorods.

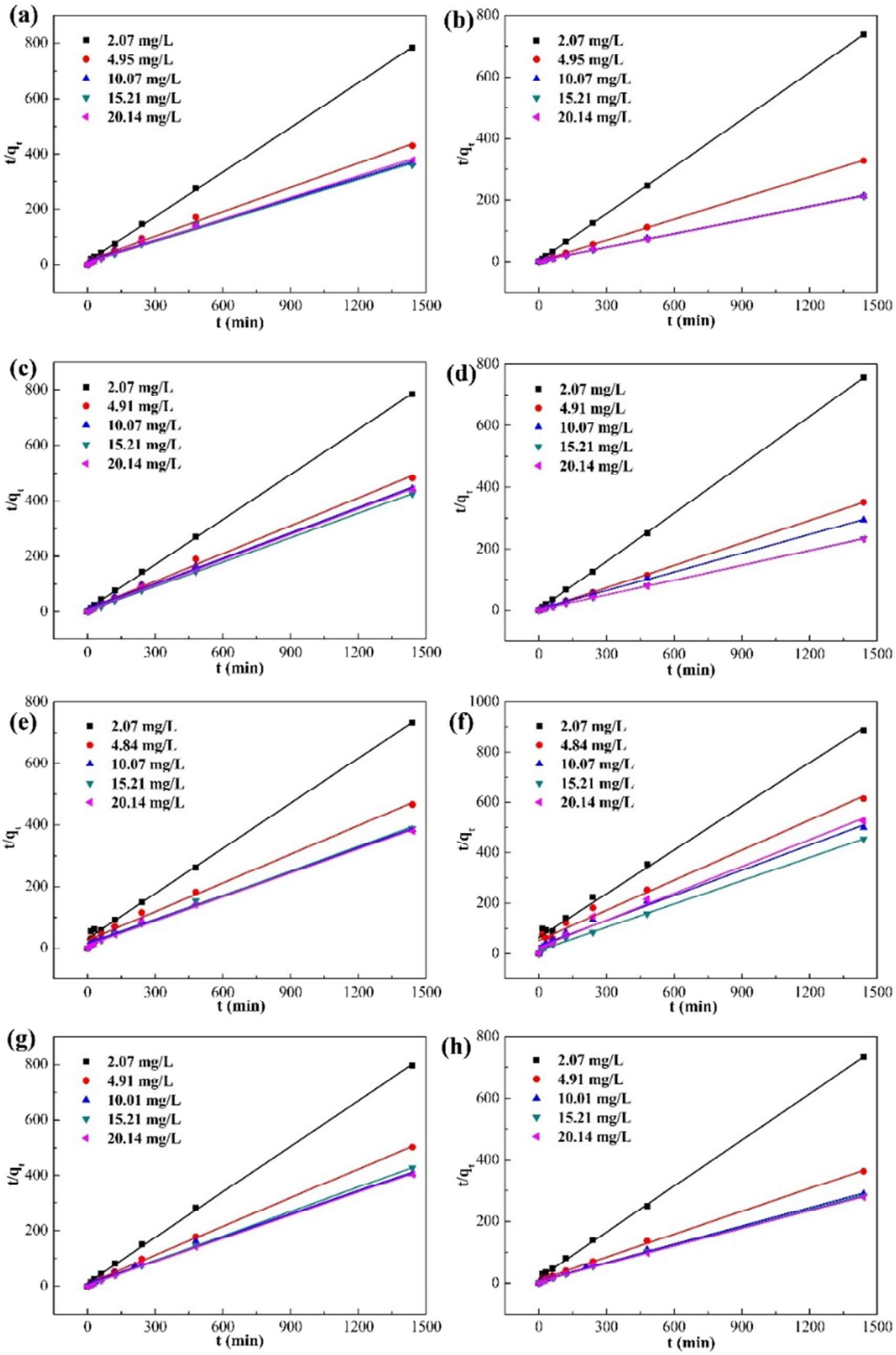

Fig. 5. Effect of initial phosphate concentrations on the adsorption kinetics of PAN/Fe_2O_3/TBAB nanofiber membranes at 23 °C. Lines represent modeled results using the pseudo-second-order equations. (a) PAN4-$Fe_2O_3$0.86-TBAB1, (b) PAN4-$Fe_2O_3$1.72-TBAB1, (c) PAN5.5-$Fe_2O_3$1.18-TBAB1, (d) PAN5.5-$Fe_2O_3$2.36-TBAB1, (e) PAN5.5-$Fe_2O_3$2.36-TBAB0.1, (f) PAN5.5-$Fe_2O_3$2.36, (g) PAN7-$Fe_2O_3$1.5-TBAB1 and (h) PAN7-$Fe_2O_3$3-TBAB1.

followed by a slower adsorption step. The kinetics correlation coefficients are summarized in Table S2 from the data fitted by the pseudo-first-order and pseudo-second-order kinetic models. The correlation coefficients (R^2) obtained according to the pseudo-second-order equation were higher than 0.9921 except for that of PAN5.5-$Fe_2O_3$2.36 nanofiber (0.9776). Based on the results of R^2, it was determined that the kinetics of the adsorption of phosphate on the PAN/Fe_2O_3/TBAB nanofiber membranes can be best described by the pseudo-second-order adsorption model, which suggests that chemisorption occurred between phosphate and the adsorbents. As shown in Table S2, the phosphate adsorption capacity at equilibrium (q_e) increased with both Fe_2O_3 and TBAB content, and the maximum value of q_e varied with the initial phosphate concentration from 2 to 20 mg/L. TBAB could not only segregate the iron oxide nanoparticles on the nanofiber surface but also synergistically improved the phosphate removal efficiency. For the same Fe_2O_3/TBAB ratio of three nanofiber membranes (i.e. PAN4-$Fe_2O_3$1.72-TBAB1, PAN5.5-$Fe_2O_3$2.36-TBAB1 and PAN7-$Fe_2O_3$3-TBAB1) with various diameter, the q_e of PAN4-$Fe_2O_3$1.72-TBAB1 was up to 6.82 mg/g for the 15 mg/L phosphate solution. This might be attributed to the smaller diameter of nanofibers leading to larger surface area and thus more active binding agents available on the nanofiber surface. Therefore, the q_e of PAN/Fe_2O_3/TBAB nanofiber membranes were determined by the Fe_2O_3 and TBAB loading and the amount of active binding agents on the nanofiber surface.

3.4. Adsorption isotherms

To further understand the adsorption mechanism, classical Langmuir and Freundlich equilibrium isotherm models (Eqs. (4) and (5)) were applied to fit the experimental data. These equilibrium models highlighted the adsorbate-adsorbent binding interaction and gave insights into possible adsorption mechanisms (Almasri et al., 2019). The Langmuir and Freundlich adsorption isotherms of PAN/Fe_2O_3/TBAB nanofiber membranes are presented in Figs. 6 and S3, respectively; the parameters for both isotherms are listed in Table 2. The correlation coefficients (R^2) obtained according to the Langmuir isotherms were more than 0.9974 except for that of PAN5.5-$Fe_2O_3$2.36 nanofibers (0.9846). Based on the results of R^2, the Langmuir isotherm best fit the experimental data for the adsorption of phosphate on the PAN/Fe_2O_3/TBAB nanofiber membranes. This might be because the Langmuir isotherm is based on monolayer adsorption onto the active sites; the active binding agents (Fe_2O_3 and TBAB) on the nanofiber surface were relatively uniform and thus a monolayer of phosphate coverage likely dominated the adsorption process. The phosphate adsorption capacity of nanofibers improved with increasing Fe_2O_3 and TBAB content and with decreasing nanofiber diameter. According to the Langmuir adsorption isotherms, the PAN4-$Fe_2O_3$1.72-TBAB1, PAN5.5-$Fe_2O_3$2.36-TBAB1 and PAN7-$Fe_2O_3$3-TBAB1 exhibited the maximum adsorption capacities of 6.9, 6.35 and 5.23 mg/g (17.05, 16.74 and 14.38 mg/g, P/active materials) for the phosphate removal, respectively.

3.5. Effect of pH

Solution pH plays an essential role in the adsorption process and particularly on the adsorption capacity; it influences not only the solution chemistry like the dominant phosphorous species, but also the surface acid-base properties of the adsorbent. Phosphate has pK_a values of 2.15, 7.2 and 12.33, and thus can exist in the form of H_3PO_4, $H_2PO_4^-$, HPO_4^{2-} or PO_4^{3-} depending on the solution pH. The fraction of species for phosphate at different pH from MATLAB simulated data are presented in Fig. 7b, while the pH in uptake experiments was varied from 2 to 13 in this work. Although the PAN4-$Fe_2O_3$1.72-TBAB1 nanofiber mat exhibited the best maximum adsorption capacity of 6.9 mg/g, the nanofiber mat was hard to peel off from aluminum foil after electrospinning and to handle as a freestanding membrane. Considering the balance of adsorption capacity and mechanical property, PAN5.5-$Fe_2O_3$2.36-TBAB1 nanofiber mat was thus chosen to study the pH effect. Fig. 7a shows the impact of the initial solution pH on phosphate removal efficiency using PAN5.5-$Fe_2O_3$2.36-TBAB1 nanofiber mat. Phosphate adsorption onto the nanofiber surface was clearly pH-dependent and tended to decrease with increasing pH, consistent with the active binding sites primarily occurring on hematite. Specifically, the effect of the initial solution pH on phosphate removal efficiency could be divided into two stages: pH-dependent continuous decline stage (pH = 2–9) and low phosphate removal efficiency stage (pH = 11–13). This is consistent with pH-edge behavior for an anion on hematite, which has a reported pH_{pzc} (pH at point of zero surface charge) ranging from 8.4 to 9.5 (Sverjensky, 2005).

When the solution pH was lower than pH_{pzc} (approx. 9), the adsorbent surface was positively charged and thus the negatively charged phosphate species like $H_2PO_4^-$ and HPO_4^{2-} preferred to adsorb. With the decrease of pH, the PAN5.5-$Fe_2O_3$2.36-TBAB1 nanofiber mat had a higher affinity toward phosphate species. The dominant mechanism of phosphate adsorption onto PAN/Fe_2O_3/TBAB nanofiber mat was assumed to be chemisorption (electrostatic attraction and ligand exchange) and the strong phosphate adsorption depended on the solution pH. At the acidic condition, the increased H^+ in solution would react with the surface hydroxyl groups on Fe_2O_3 to form some protonated hydroxyl groups. The electrostatic attraction existed in both protonated hydroxyl group of Fe_2O_3 particles and ammonium ions of TBAB on the nanofiber surface with phosphate for adsorption. Besides, inner-sphere complexation or ligand exchange could readily occur (pH 4 and 5) between $H_2PO_4^-$ and the surface OH^- groups to form complexation like Fe-H_2PO_4. This exchange reaction could be inferred from the increased solution equilibrium pH (5.2 and 5.73) after adsorption showed in Fig. 7a, which is consistent with hydroxide ion release. Notably, phosphate removal capacity of the PAN5.5-$Fe_2O_3$2.36-TBAB1 nanofiber mat was up to 8.89 and 8.76 mg/g (23.44 and 23.1 mg/g, P/active materials) at pH 2 and 3, respectively.

When the solution pH was higher than pH_{pzc}, the adsorbent surface was negatively charged, which leads to the formation of deprotonated hydroxyl groups. The phosphate adsorption onto hematite was mainly affected by the electrostatic repulsion, which increases with increasing pH. The active binding agents Fe_2O_3 on the nanofiber surface are deprotonated and negatively charged along with phosphate species (Li et al., 2016). Instead, we attribute most phosphate uptake at higher pH values above the pH_{pzc} of hematite to favorable electrostatic attraction of positively charged quaternary ammonium ions of TBAB with phosphate.

3.6. Desorption and reusability

It is well known that in actual wastewater remediation applications, the reuse of adsorbent could improve the adsorption efficiencies and reduce the costs. Hence, the adsorbent reusability was examined by determining how much of the original adsorption capacity was retained after each regeneration cycle. Fig. 8 shows the phosphate adsorption capacity of PAN5.5-$Fe_2O_3$2.36-TBAB1 nanofiber mat at pH 3 and 5 through 5 consecutive cycles via the alkaline regeneration method. The result of cycle 0 was assigned to the phosphate adsorption capacity of the original as-spun PAN5.5-$Fe_2O_3$2.36-TBAB1 nanofiber mat at pH 3 and 5. As shown in Fig. 8, the phosphate adsorption capacity of the original electrospun PAN5.5-$Fe_2O_3$2.36-TBAB1 nanofiber mat decreased after each regeneration cycle, but the degree at which it decreased was affected by the pH of the initial phosphate solution. The reusability of the PAN5.5-$Fe_2O_3$2.36-TBAB1 nanofiber mat at pH 3 was better than that of the nanofiber mat at pH 5. The amount of phosphate adsorption capacity for the 1st regeneration cycle maintained at 80.6% and 50.9% of the original adsorption capacity at pH 3 and 5, respectively. It is worth mentioning that the phosphate adsorption capacity of PAN5.5-$Fe_2O_3$2.36-TBAB1 nanofiber mat at pH 3 after 5 cycles of regeneration could still reach 4.94 mg/g (56.4% of that at cycle 0). In contrast, the phosphate adsorption capacity at pH 5 after 5 cycle regeneration was only 1.01 mg/g (17.7% of that at

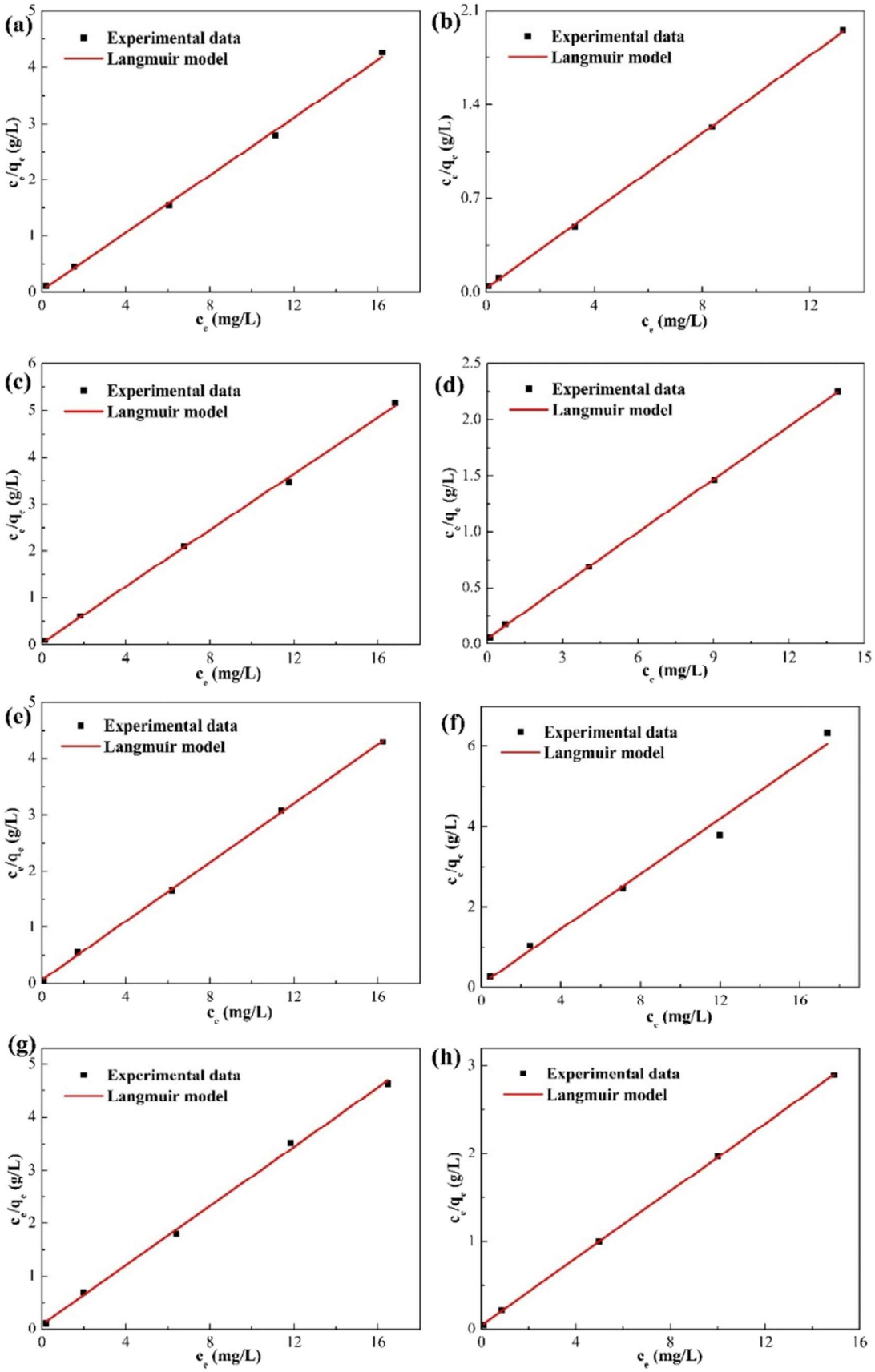

Fig. 6. Langmuir adsorption isotherms for the adsorption of PAN/Fe_2O_3/TBAB nanofiber membranes. (a) PAN4-$Fe_2O_3$0.86-TBAB1, (b) PAN4-$Fe_2O_3$1.72-TBAB1, (c) PAN5.5-$Fe_2O_3$1.18-TBAB1, (d) PAN5.5-$Fe_2O_3$2.36-TBAB1, (e) PAN5.5-$Fe_2O_3$2.36-TBAB0.1, (f) PAN5.5-$Fe_2O_3$2.36, (g) PAN7-$Fe_2O_3$1.5-TBAB1 and (h) PAN7-$Fe_2O_3$3-TBAB1.

Table 2
The parameters for the Langmuir and Freundlich isotherms and the correlation coefficients for the phosphate adsorption of PAN/Fe_2O_3/TBAB nanofiber membranes.

Adsorbents	Langmuir isotherm			Freundlich isotherm		
	q_{max} (mg/g)	K_L	R^2	n	K_F	R^2
PAN4-$Fe_2O_3$0.86-TBAB1	3.91	7.496	0.9979	5.798	2.662	0.8274
PAN4-$Fe_2O_3$1.72-TBAB1	6.9	5.111	0.9997	4.115	4.233	0.8397
PAN5.5-$Fe_2O_3$1.18-TBAB1	3.328	7.37	0.9988	7.654	2.452	0.87
PAN5.5-$Fe_2O_3$2.36-TBAB1	6.351	3.138	0.9999	4.099	3.714	0.8893
PAN5.5-$Fe_2O_3$2.36-TBAB0.1	3.819	4.469	0.9994	7.534	2.754	0.9556
PAN5.5-$Fe_2O_3$2.36	2.908	4.733	0.9846	5.998	1.946	0.854
PAN7-$Fe_2O_3$1.5-TBAB1	3.583	3.171	0.9974	6.396	2.424	0.9164
PAN7-$Fe_2O_3$3-TBAB1	5.231	4.256	0.9999	5.259	3.41	0.8795

cycle 0). This pH effect on the reusability might be explained by the difference of adsorption mechanism changing from the pH of phosphate solution. The electrostatic attraction dominated in adsorption mechanism at pH 3, while the adsorption mechanism was a combination of electrostatic attraction and ligand exchange at pH 5. Compared to the electrostatic attraction, the complex Fe-H_2PO_4 formed by ligand exchange was relatively difficult to desorb through the alkaline regeneration method.

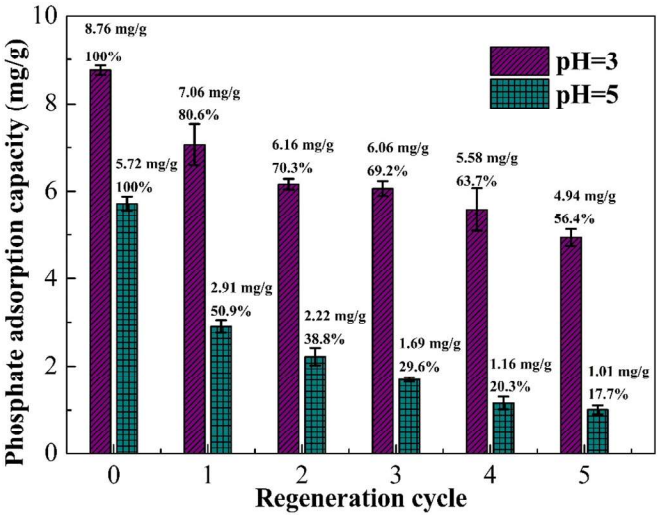

Fig. 8. The phosphate adsorption capacity of PAN5.5-$Fe_2O_3$2.36-TBAB1 nanofiber mat with 5 cycles regeneration using 1 M NaOH solution. Initial phosphate concentration 10 mg/L, pH 3 and 5, contact time 24 h, adsorbent dosage 1 g/L.

4. Conclusion

Surfactant-mediated electrospinning of PAN/Fe_2O_3/TBAB nanofiber membranes was designed and successfully prepared via a one-pot electrospinning technique. PAN concentration and PAN/Fe_2O_3 ratio were systematically varied according to the design of experiment to elucidate their effect on the nanofiber diameter and bead density. The viscosity of the solution, largely dictated by the PAN concentration, was the main factor in controlling the nanofiber diameter. The higher PAN concentration would lead to higher nanofiber diameter and lower bead density. Both SEM and TEM images clearly showed the Fe_2O_3 enriched at the nanofiber surface. The adsorption of phosphate onto the PAN5.5-$Fe_2O_3$2.36-TBAB1 nanofiber membrane followed the pseudo-second-order kinetic model and fitted well with the Langmuir adsorption isotherm with an adsorption capacity of 8.76 mg/g (23.1 mg/g, P/active materials) at pH 3. The phosphate adsorption was pH-dependent and tended to decrease with increasing pH. At the low initial solution pH of 3, the PAN/Fe_2O_3/TBAB nanofiber membranes displayed good reusability for phosphate removal, maintaining 56.4% of its initial adsorption capacity (i.e. 4.94 mg/g). The adsorption mechanism was mainly derived from the chemisorption of Fe_2O_3 nanoparticles at the surface of the nanofibers and partly originated from anion exchange of TBAB.

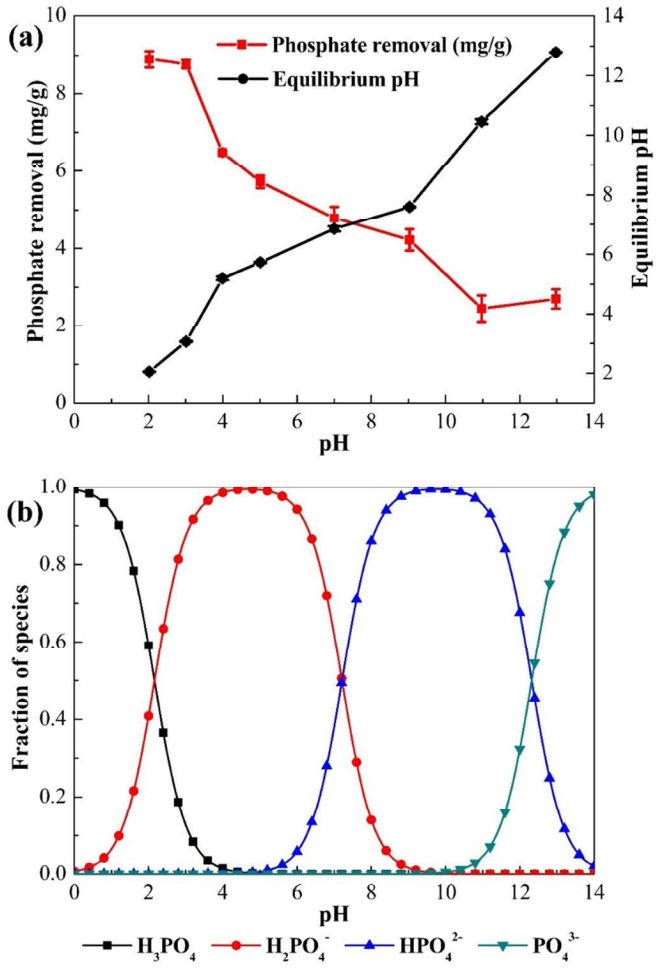

Fig. 7. (a) Effect of the initial solution pH on phosphate removal efficiency using PAN5.5-$Fe_2O_3$2.36-TBAB1 nanofiber mat and (b) Fraction of species for phosphate at different pH from MATLAB simulated data. Initial phosphate concentration 10 mg/L, contact time 24 h, $T = 23$ °C, adsorbent dosage 1 g/L.

CRediT authorship contribution statement

Chengshuang Wang: Conceptualization, Methodology, Data curation, Investigation, Visualization, Writing – original draft. **Sooyoun Yu:** Methodology, Data curation, Investigation, Visualization, Writing – original draft. **David M. Cwiertny:** Formal analysis, Methodology, Writing – review & editing. **Yadong Yin:** Supervision, Resources, Writing – review & editing. **Nosang V. Myung:** Conceptualization, Methodology, Supervision, Project administration, Resources, Funding acquisition, Writing – review & editing.

Declaration of competing interest

The authors declare that they have no known competing financial interests or personal relationships that could have appeared to influence the work reported in this paper.

Acknowledgments

We acknowledge the financial support from National Science Foundation (CBET # 1804757). C.S. Wang also likes to acknowledge the financial support from the National Natural Science Foundation of

China (Grant No. 51903217), the Initial Scientific Research Foundation of Yancheng Institute of Technology (Grant No. KJC2014001), and the Jiangsu Overseas Research & Training Program for University Prominent Young & Middle-aged Teachers and Presidents for support.

Appendix A. Supplementary data

Supplementary data to this article can be found online at https://doi.org/10.1016/j.scitotenv.2021.145364.

References

Almasri, D.A., Saleh, N.B., Atieh, M.A., McKay, G., Ahzi, S., 2019. Adsorption of phosphate on iron oxide doped halloysite nanotubes. Sci. Rep. 9, 3232.

Bacelo, H., Pintor, A.M.A., Santos, S.C.R., Boaventura, R.A.R., Botelho, C.M.S., 2020. Performance and prospects of different adsorbents for phosphorus uptake and recovery from water. Chem. Eng. J. 381, 122566.

Bhardwaj, N., Kundu, S.C., 2010. Electrospinning: a fascinating fiber fabrication technique. Biotechnol. Adv. 28, 325–347.

Chen, H., Huang, M., Liu, Y., Meng, L., Ma, M., 2020. Functionalized electrospun nanofiber membranes for water treatment: a review. Sci. Total Environ. 739, 139944.

Chisca, S., Barzic, A.I., Sava, I., Olaru, N., Bruma, M., 2012. Morphological and rheological insights on polyimide chain entanglements for electrospinning produced fibers. J. Phys. Chem. B 116, 9082–9088.

Cui, Q., Xu, J., Wang, W., Tan, L., Cui, Y., Wang, T., et al., 2020. Phosphorus recovery by core-shell γ-Al_2O_3/Fe_3O_4 biochar composite from aqueous phosphate solutions. Sci. Total Environ. 729, 138892.

Ding, B., Yu, J., 2014. Electrospun Nanofibers for Energy and Environmental Applications. Springer, Berlin, Heidelberg, Germany.

Dodds, W.K., Bouska, W.W., Eitzmann, J.L., Pilger, T.J., Pitts, K.L., Riley, A.J., et al., 2009. Eutrophication of US freshwaters: analysis of potential economic damages. Environ. Sci. Technol. 43, 12–19.

Doolittle, P., 2014. Ascorbic Acid Method for Phosphorus Determination. University of Wisconsin-Madison.

Fang, L., Wu, B., Lo, I.M.C., 2017. Fabrication of silica-free superparamagnetic ZrO_2@Fe_3O_4 with enhanced phosphate recovery from sewage: performance and adsorption mechanism. Chem. Eng. J. 319, 258–267.

Greenstein, K.E., Myung, N.V., Parkin, G.F., Cwiertny, D.M., 2019. Performance comparison of hematite (α-Fe_2O_3)-polymer composite and core-shell nanofibers as point-of-use filtration platforms for metal sequestration. Water Res. 148, 492–503.

Lalley, J., Han, C., Li, X., Dionysiou, D.D., Nadagouda, M.N., 2016. Phosphate adsorption using modified iron oxide-based sorbents in lake water: kinetics, equilibrium, and column tests. Chem. Eng. J. 284, 1386–1396.

Li, M., Liu, J., Xu, Y., Qian, G., 2016. Phosphate adsorption on metal oxides and metal hydroxides: a comparative review. Environ. Rev. 24, 319–332.

Li, R., Wang, J.J., Gaston, L.A., Zhou, B., Li, M., Xiao, R., et al., 2018. An overview of carbothermal synthesis of metal-biochar composites for the removal of oxyanion contaminants from aqueous solution. Carbon 129, 674–687.

Li, S., Huang, X., Liu, J., Lu, L., Peng, K., Bhattarai, R., 2020. PVA/PEI crosslinked electrospun nanofibers with embedded $La(OH)_3$ nanorod for selective adsorption of high flux low concentration phosphorus. J. Hazard. Mater. 384, 121457.

Liao, Y., Loh, C.-H., Tian, M., Wang, R., Fane, A.G., 2018. Progress in electrospun polymeric nanofibrous membranes for water treatment: fabrication, modification and applications. Prog. Polym. Sci. 77, 69–94.

Liu, J., Wu, Y., Wu, C., Muylaert, K., Vyverman, W., Yu, H.-Q., et al., 2017. Advanced nutrient removal from surface water by a consortium of attached microalgae and bacteria: a review. Bioresour. Technol. 241, 1127–1137.

Lofrano, G., Carotenuto, M., Libralato, G., Domingos, R.F., Markus, A., Dini, L., et al., 2016. Polymer functionalized nanocomposites for metals removal from water and wastewater: an overview. Water Res. 92, 22–37.

Nguyen, T.A.H., Ngo, H.H., Guo, W.S., Zhang, J., Liang, S., Lee, D.J., et al., 2014. Modification of agricultural waste/by-products for enhanced phosphate removal and recovery: potential and obstacles. Bioresour. Technol. 169, 750–762.

Park, J.Y., Lee, I.H., Bea, G.N., 2008. Optimization of the electrospinning conditions for preparation of nanofibers from polyvinylacetate (PVAc) in ethanol solvent. J. Ind. Eng. Chem. 14, 707–713.

Peter, K.T., Vargo, J.D., Rupasinghe, T.P., De Jesus, A., Tivanski, A.V., Sander, E.A., et al., 2016. Synthesis, optimization, and performance demonstration of electrospun carbon nanofiber-carbon nanotube composite sorbents for point-of-use water treatment. ACS Appl. Mater. Inter. 8, 11431–11440.

Peter, K.T., Johns, A.J., Myung, N.V., Cwiertny, D.M., 2017. Functionalized polymer-iron oxide hybrid nanofibers: electrospun filtration devices for metal oxyanion removal. Water Res. 117, 207–217.

Peter, K.T., Myung, N.V., Cwiertny, D.M., 2018. Surfactant-assisted fabrication of porous polymeric nanofibers with surface-enriched iron oxide nanoparticles: composite filtration materials for removal of metal cations. Environ. Sci.: Nano 5, 669–681.

Singh, N.B., Nagpal, G., Agrawal, S., Rachna, 2018. Water purification by using adsorbents: a review. Environ. Technol. Inno. 11, 187–240.

Suja, P.S., Reshmi, C.R., Sagitha, P., Sujith, A., 2017. Electrospun nanofibrous membranes for water purification. Polym. Rev. 57, 467–504.

Sverjensky, D.A., 2005. Prediction of surface charge on oxides in salt solutions: revisions for 1:1 (M+L−) electrolytes. Geochim. Cosmochim. Acta 69, 225–257.

Tan, X.-f., Liu, Y.-g., Gu, Y.-l., Xu, Y., Zeng, G.-m., Hu, X.-j, et al., 2016. Biochar-based nanocomposites for the decontamination of wastewater: a review. Bioresour. Technol. 212, 318–333.

Xia, W.-J., Yu, L.-Q., Zhang, Q., Zhao, Y.-H., Xiong, J.-R., Zhu, X.-Y., et al., 2020. Conversion of municipal wastewater-derived waste to an adsorbent for phosphorus recovery from secondary effluent. Sci. Total Environ. 705, 135959.

Xue, J., Xie, J., Liu, W., Xia, Y., 2017. Electrospun nanofibers: new concepts, materials, and applications. Acc. Chem. Res. 50, 1976–1987.

Xue, J., Wu, T., Dai, Y., Xia, Y., 2019. Electrospinning and electrospun nanofibers: methods, materials, and applications. Chem. Rev. 119, 5298–5415.

Yu, S., Myung, N.V., 2018. Minimizing the diameter of electrospun polyacrylonitrile (PAN) nanofibers by design of experiments for electrochemical application. Electroanal. 30, 2330–2338.

Zhao, X., Lv, L., Pan, B., Zhang, W., Zhang, S., Zhang, Q., 2011. Polymer-supported nanocomposites for environmental application: a review. Chem. Eng. J. 170, 381–394.

Zhao, J., Lu, Z., He, X., Zhang, X., Li, Q., Xia, T., et al., 2017. One-step fabrication of $Fe(OH)_3$@cellulose hollow nanofibers with superior capability for water purification. ACS Appl. Mater. Inter. 9, 25339–25349.

Zhao, G., Huang, X., Tang, Z., Huang, Q., Niu, F., Wang, X., 2018. Polymer-based nanocomposites for heavy metal ions removal from aqueous solution: a review. Polym. Chem. 9, 3562–3582.